New generation graphenes in cement-based materials: Production, property enhancement, and life cycle analysis

Sahil Surehali[1], Sayee Srikarah Volaity[1], Aswathy Simon[1], Ranjith Divigalpitiya[2], Aditya Kumar[3], Narayanan Neithalath[4]*

Abstract:

Several studies have explored the use of graphene to improve the properties of cement-based materials. However, most commercially available graphenes are expensive, not amenable to mass production, and have high embodied energy and emissions, making their use in concrete less attractive, despite the beneficial mechanical property attributes. This paper discusses the use of two novel graphene types—fractal graphene (FG) and reactive graphene (RG)—obtained through a cost-effective and scalable detonation synthesis, in cement-based materials. FG and RG are sheets containing 6-10 layers, with lateral dimensions of 20-50 nm and z-axis thickness of <5 nm. RG is functionalized with carboxylic groups. An ultrasonication process is employed to ensure dispersion of graphene particles in aqueous solutions. Both FG and RG, when added at very small dosages (≤0.04% by mass of cement), enhance the compressive strength of cement mortars by >70% at early ages and up to 20% at later ages. The beneficial effect of functionalization results in better performance for RG-modified mixtures, even at dosages as low as 0.02%. Concomitant enhancements in heat of hydration, hydrate formation, and rheological response are observed. A significant reduction in porosity and critical pore size (by 50% or more) promises significantly improved concrete durability, and thus reduced life-cycle costs. A comparative life cycle analysis (LCA) is used to show that FG- and RG-modified mortars have normalized (by the 28-d strength) energy demand and global warming potential (GWP) that is up to 15% lower than those of conventional mortars. Overall, this study shows that FG and RG manufactured through scalable, cost-, energy-, and CO_2-efficient detonation synthesis, can beneficially impact the engineering and environmental performance of concretes.

Keywords: graphene; compressive strength; hydration kinetics; pore structure; life cycle analysis

[1] Graduate student, School of Sustainable Engineering and Built Environment, Arizona State University, Tempe AZ 85287

[2] Chief Science Officer, HydroGraph, ON Canada N6G 4X8

[3] Associate Professor, Department of Materials Science and Engineering, Missouri University of Science and Technology, Rolla, MO 65409

[4] Professor, School of Sustainable Engineering and Built Environment, Arizona State University, Tempe AZ 85287; Corresponding author: e-mail: Narayanan.Neithalath@asu.edu

1. Introduction

Graphene, a two-dimensional nanomaterial, has gained immense popularity since its discovery, mainly due to its very high tensile strength (130 GPa; for comparison, the tensile strength of steel is < 1 GPa) and elastic modulus (1.1 TPa). These properties have made the use of graphene (and its derivatives; see below) in cement-based materials attractive. Indeed, several studies have been carried out in the recent past aiming to improve the properties and performance of cementitious materials through the incorporation of graphene and its derivatives [1–6].

Graphene is a single atom thick planar sheet of sp^2-bonded carbon atoms [7,8]. It exists in diverse forms, with the prominent types being graphene nanoplatelets (GNPs), graphene oxide (GO), and reduced graphene oxide (rGO). GNPs are composed of graphene sheets, typically ranging between 10 and 100 layers. GO features numerous hydroxyl, carboxyl, epoxy, and other functional groups on the graphene surface [9]. rGO is synthesized by partially reconstituting the graphene lattice by removing the oxidized functional groups via reducing agents [10]. GNPs are difficult to disperse in aqueous solutions; instead, they form entangled clumps because of the highly attractive Van der Waals forces between the platelets [11]. In contrast, the grafted oxygen functional groups in GO and rGO can reduce the Van der Waals forces and increase electrostatic repulsion between GO sheets, making dispersion easier. This enhanced dispersion of GO has been exploited by several studies, demonstrating that even small amounts of GO, used as an additive, can improve both early- and later-age properties of cementitious materials [9,12–14]; even though the use of GNPs has also been reported [15–17]. As expected, the reinforcing efficiency of graphene (GNP, or GO, or rGO) in cementitious mixtures is influenced by graphene's physicochemical characteristics (sheet size, oxygen content, functional group, layer thickness, and number of layers) and its properties (tensile strength and Young's modulus), along with the characteristics of the mixture components and the preparation method of GO-cement composites [1–6]. By and large, properly proportioned cementitious materials, containing a small amount of graphene, demonstrate superior mechanical and durability properties [18–21].

Several methods have been put forth for the synthesis of graphene. The scale of production as well as the characteristics of the final product—including the geometry and size of graphene particulates, and the thickness and number of layers—are dictated by the chosen synthesis technique. The most common top-down methods of graphene production from graphite include mechanical and chemical exfoliation, and chemical oxidation-reduction [22–24]. While these methods are suitable for large-scale production of graphene, the difficulty in obtaining the desired particle size and shape consistently is a significant drawback [25]. Furthermore, the energy and environmental impacts of many of these manufacturing processes are non-trivial. For example, GO is generally made using modified Hummer's method; here, graphite powder is oxidized with powerful chemical oxidants and concentrated acids, resulting in formation of undesirable by-products [26]. To make rGO, the resulting GO must be chemically reduced using potent reducing agents. It has also been reported that the top-down approaches for producing graphene could have a carbon footprint of up to ~620 g CO_2-eq per g of graphene produced [27,28]. The bottom-up methods use organic compounds as precursors for processes such as chemical vapor deposition, organic synthesis, and pyrolysis [29]. Many of these processes are expensive (at \$70-\$200 kg^{-1} [30]) and not amenable for high volume synthesis in a CO_2-and-energy efficient manner. Recently, flash joule heating has been proposed as a method to convert carbon-rich natural and waste materials (e.g., biomass, crop residues, etc.) to flash graphene; but, this process, generally, produces graphene of inferior quality, with large fractions of defects, contamination, and oxidized fractions [25,27,31].

The foregoing discussion reinforces the need to develop a more efficient, scalable, economic process to produce graphene of high quality. This is imperative for the continued use of graphene in cement-based materials, which demand high volumes at low cost. In this paper, we focus on novel, high-quality graphene materials synthesized by Hydrograph, through controlled detonation of oxygen/acetylene mixtures [30]. The synthesis method has been scaled up in a modular system with a footprint of only 4 m^2 to produce >10 metric tons of graphene annually at one of the lowest capex costs per metric ton of graphene [32]. This study uses two types of the so-produced graphene—termed as fractal and reactive graphenes (FG and RG)—for the first time in cementitious mixtures. Emphasis is given to study the mixtures' hydration characteristics, and early- and later-age property enhancement attained using very small amounts ($\leq$ 0.04% by mass of cement) of graphene. The differences between FG and RG as compared to GNPs, GO, and rGO are in their methods of production, particle sizes, and purity—as explained in the forthcoming sections. It is worth pointing out that both FG and RG remain unexplored in the realm of cementitious materials; hence this study aims to bridge this gap by examining and delineating the distinct characteristics of FG and RG in contrast to their commonly-used counterparts, namely GNP, GO, and rGO. Through comparative evaluation of properties of various graphene-incorporated cementitious composites, this study seeks to highlight the nuanced differences and potential advantages FG and RG may offer. The lower carbon- and energy-impacts of FG and RG as opposed to GNP, GO, and rGO, which are established in this work through a comparative life cycle analysis (LCA), in addition to their lower production cost than currently available high-purity graphenes, are expected to positively contribute to their acceptability in cementitious materials applications.

2. Graphene production and its characteristics

2.1 Synthesis of fractal and reactive graphenes (FG, RG)

Graphene used in this study is produced through a novel, cost-effective, eco-friendly, one-step method that involves controlled detonation of an acetylene-oxygen mixture in a chamber under a spark of 10 kV from an industrial step-up transformer. Detonation synthesis is a simple, fast, catalyst-free, and economically viable method to produce high-quality graphene [30,33]. The experimental set up for detonation synthesis and a process flow diagram are shown in supplementary information (SI). The detonation process produces high temperatures (~3000 K) and pressures ($\leq$300 psi), along with a supersonic detonation (combustion) wave that induces the conversion of acetylene into free carbon atoms, which subsequently condense into carbon nanoparticles upon cooling. The powder aggregates quickly to form an aerosol gel inside the container to yield a fractal structure called FG aggregate [34]. This process does not produce carbonaceous soot, because the detonation temperature is much higher than the temperature for soot production. All production sub-processes are carried out in the gas phase without any catalysts, resulting in production of elementally-pure graphene with carbon content >99% with high batch-to-batch consistency [30]. Reactive graphene (RG) is produced from fractal graphene by functionalizing it with COOH groups on the surface alone using a Fenton oxidation process [35], thereby making it suitable for dispersion. Fenton oxidation is defined as the oxidation of organic materials by Fenton's reagent (hydrogen peroxide and Fe^{2+}). Compared to the commonly used Hummer's method to produce GO, while the Fenton process has similar efficiency [36], the preferential reaction of Fenton's reagent with the edges of FG leads to the formation of less defective oxides (RG, in this case). Figure 1 shows a comparison between the structure of conventional GO and rGO [37], and FG and RG that are used in this study. While traditional GO may contain multiple types of oxygen-containing moieties such as hydroxyl, carbonyl, carboxylic, and epoxide groups attached to both

surfaces [38,39], RG contains only carboxylic groups. For more description on the synthesis procedure, readers are referred to [30,34,35].

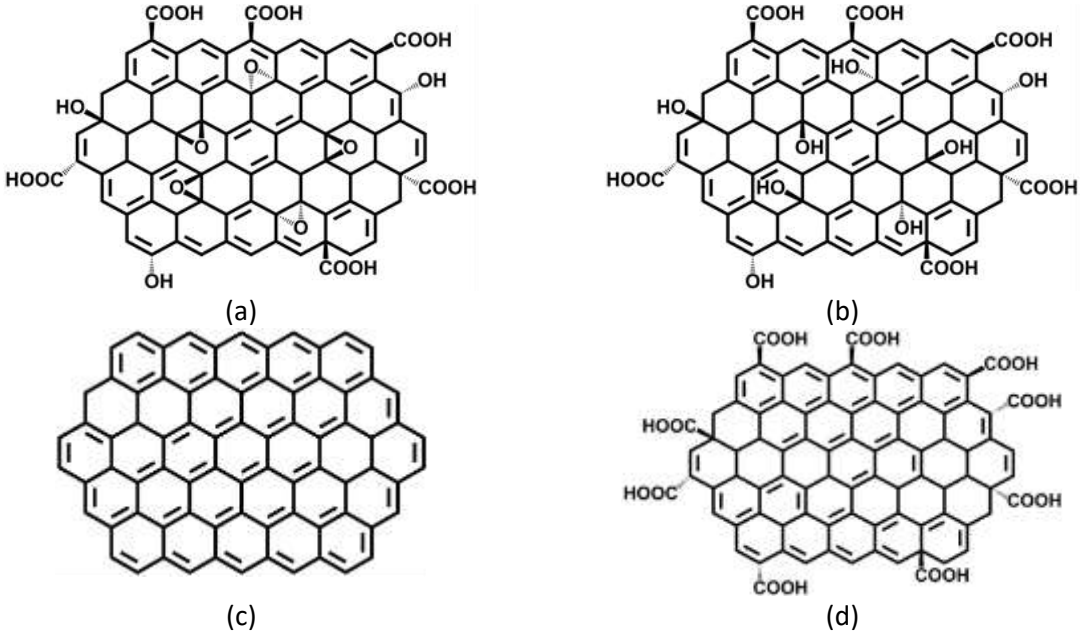

Figure 1: Structure of (a) GO and (b) rGO [37]; and (c) FG and (d) RG

The above-mentioned detonation synthesis process boasts a significant advantage in energy efficiency over other methods of producing graphene. Unlike other graphene manufacturing techniques, the detonation-based process is devoid of any rotating machinery, consumes minimal energy, and operates without solvents, thereby eliminating greenhouse gas (GHG) emissions. The process leverages the exothermic reaction between acetylene and oxygen, which requires substantially less energy per kg of graphene compared to traditional manufacturing techniques such as ultrasonic exfoliation, Hummer's method, and flash Joule heating, all of which are discussed in Section 5. In addition to very low energy demand, the detonation synthesis process does not use water, while producing high-value syngas as the sole by-product, which can be effectively captured and repurposed for diverse applications. The Fenton process that converts FG to RG eliminates the disadvantages of conventional GO production techniques (e.g., Hummer's method) because: Fe and H_2O_2 are cheap and environmentally innocuous; H_2O_2 activation occurs at ambient temperature and pressure; and the reactions do not generate toxic gases [36]. Thus, the manufacturing process of FG and RG are not just more sustainable but also significantly more inexpensive compared to traditional processes.

2.2 Characteristics of FG and RG

The aerosol gel (FG) collected from the process has a tapped bulk density < 100 mg.cm^{-3}. As described earlier, RG is essentially FG functionalized with COOH groups. The chemical composition of FG and RG are provided in Table 1, along with those of GO and rGO, to demonstrate the purity of the graphenes used in this study.

Table 1: Chemical composition of fractal graphene (FG), reactive graphene (RG), graphene oxide (GO) and reduced graphene oxide (rGO) (Note: Data for FG and RG from [35], and for GO and rGO from [26]). The composition of rGO could vary significantly based on the type of reducing agent used ([39]).

Element	Fractal graphene (FG)	Reactive graphene (RG)	Graphene oxide (GO)	Reduced graphene oxide (rGO)
C%	99.2	90.1	44	56
O%	0.7	8.2	53	41
H%	0.1	1.7	3	3

Transmission electron microscopy (TEM) images of FG are shown in Figure 2, which depict its geometric attributes, with lateral dimensions of 20-50 nm, and a z-axis dimension of <5 nm. On average, each particle contains 6-10 layers. The TEM images also show some crumpling of layers consistent with the morphology of graphene synthesized using other methods [34]. The dimensions of FG produced by detonation synthesis are much smaller than those of GOs and GNPs, which is typically on the order of 100 nm [40]. Experimental specific surface area (SSA) of graphene is determined to be ~200 m^2g^{-1}, which is an order of magnitude lower than the theoretical SSA of 2630 m^2g^{-1} for isolated graphene sheets [41–43] obtained under a rigorous dispersion scheme (e.g., ultrasonication).

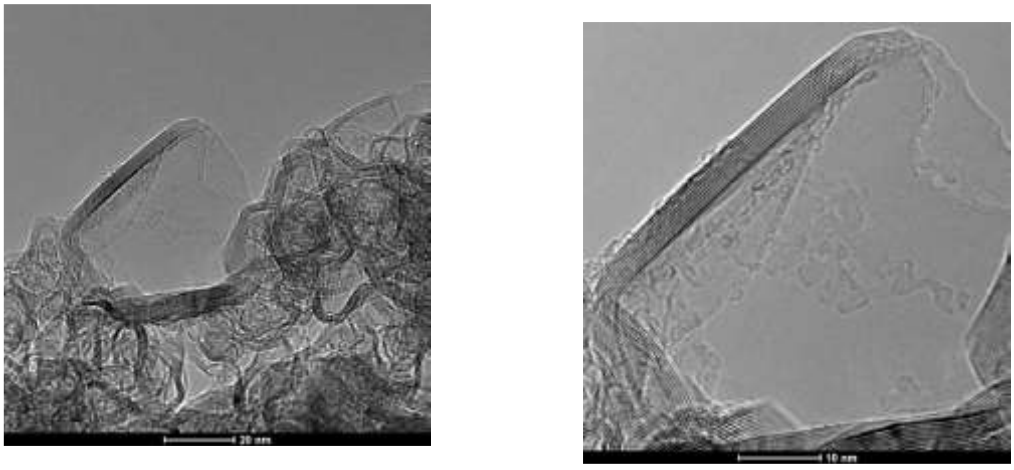

(a) (b)

Figure 2: (a) and (b) Transmission electron micrographs of fractal graphene (FG). Reactive graphene consists of chemical modification of FG by functionalizing it, and does not change the physical attributes such as shape and size.

The x-ray diffraction (XRD) spectra of FG and RG are shown in Figure 3(a). The most intense peak (002) is centered at ~26°, implying an interplanar spacing (d) of 0.341 nm, which is in good agreement with graphenes synthesized using other methods [44,45]. Figure 3(b) shows the Raman spectra of FG and RG, measured at an excitation wavelength of 514 nm. The G-band is the primary mode in graphene, representing the planar configuration of sp^2-bonded carbon in graphene. The G-band position also indicates the number of layers (z-axis dimension), with a shift to the right indicating more number of layers. Shifts in the G-band position also could indicate doping. D-band or defect-band indicates the partially disordered structures of the sp^2 domains, while 2D-band which a strong band in graphene is more sensitive to graphene folding, and is used to probe graphene thickness [46]. Characteristic G- and 2D-bands are observed in Figure 3(b) at 1584 cm^{-1} and 2690 cm^{-1}. The nanoscale lateral dimensions of platelets lead to a high fraction of defect edge sites, which enhances the intensity of the D-band observed at 1328 cm^{-1}. Both the XRD and Raman spectra are very similar for FG and RG.

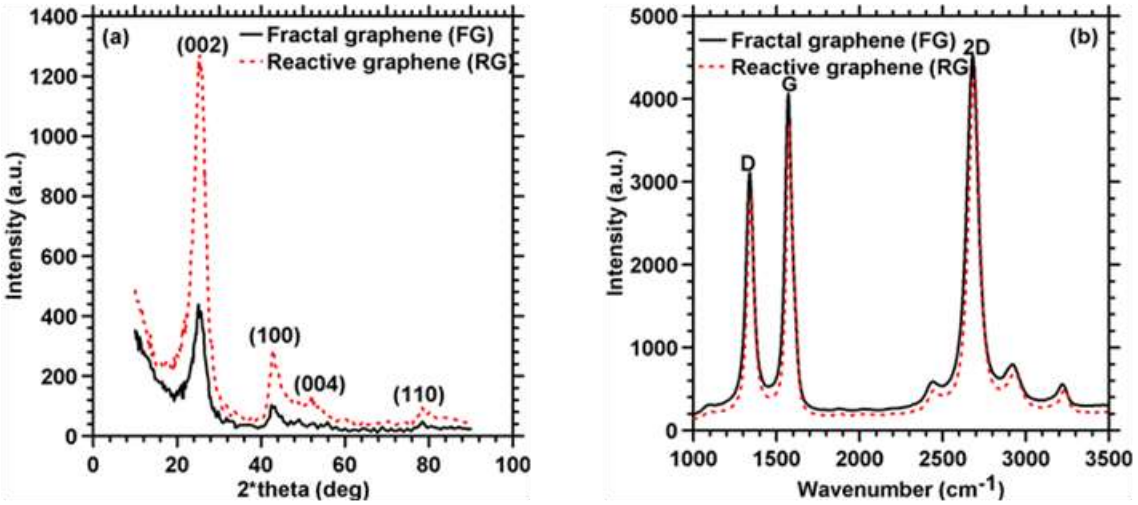

(a) (b)

Figure 3: (a) X-ray diffraction spectra, and (b) Raman spectra of fractal and reactive graphenes [35].

3. Cementitious mixtures and experimental program

3.1 Materials and mixtures

This study utilized Type I/II ordinary Portland cement (OPC) conforming to ASTM C 150 provided by Salt River Materials Group (Phoenix Cement) to prepare the cement pastes and mortars. The chemical composition of OPC is summarized in Table 2. The median particle size (d_{50}) of OPC was determined as 15.2 µm using laser diffraction. The specific gravity was determined using a gas pycnometer in accordance with ASTM D 5550. These parameters are also shown in Table 2.

Table 2: Chemical composition and physical properties of ordinary Portland cement used in the study.

Chemical composition								Physical properties	
SiO_2 (%)	Al_2O_3 (%)	SO_3 (%)	Fe_2O_3 (%)	MgO (%)	Na_2O (%)	K_2O (%)	CaO (%)	LOI* (%)	Specific gravity
21.3	3.78	2.88	3.75	1.77	0.25	0.17	63.8	1.34	3.20
*Loss on Ignition									

The cement pastes used in this study were prepared at a water-to-cement ratio (w/c) of 0.40. Different graphene dosages from 0 to 0.10% by mass of cement were initially used to proportion the cement pastes. Based on the cement content and w/c, the amount of graphene needed for a paste with a certain graphene content was determined, and dispersed in water using a procedure described in the following section. Compressive strengths of mortars (50% sand by mass of the binder) were determined at 1-, 3-, and 7-days to refine (optimize) the graphene dosages for further materials characterization and testing. No chemical admixtures were used since the objective is to understand the influence of graphene in cement pastes, and admixtures have the propensity to interact with the functional groups in graphene.

3.2 Dispersion of FG and RG in water

It is important that nanosized graphene is uniformly dispersed in the mixing water, to ensure adequate dispersibility in a cementitious matrix. The very small size and attractive Van der Waals forces result

in agglomeration of nanosized particles, thereby rendering them less effective in enhancing the properties of cementitious materials. To prepare a well-dispersed graphene suspension, graphene was first homogenized with de-ionized (DI) water for 2 min. Next, the beaker with the solution was moved into a cell where the suspension underwent ultrasonication at a frequency of 40 kHz (and 400 W power) for 3 h. Care was taken to prevent water loss during ultrasonication, and to avoid overheating of the solution. While 3 h of ultrasonication is used in this study, this time can be further reduced to 15-30 min with a modified procedure featuring the use of a chemical admixture (superplasticizer); this procedure will be discussed in our companion studies. Figures 4(a)-(c) show aqueous dispersions of graphene without and with ultrasonication, clearly demonstrating the effect of ultrasonication on particles' dispersion.

Graphene-water suspension was characterized by UV-Vis spectrometry using a Hach DR6000 UV/VIS Spectrophotometer. The measurement was performed in a wavelength range of 250-1100 nm; here, DI water was used for baseline correction. To further confirm the stability of graphene suspensions as a function of time, the experiments were also performed after 1-, 3-, and 7-d of dispersion. The UV-Vis absorbance spectra for solutions containing FG and RG are shown in Figure 4(d) and (e) respectively. It can be seen that the absorbance peak of the UV-Vis spectra of the suspension does not change noticeably even after 7-d, showing that the dispersion process used in this study can produce stable FG and RG suspensions that can be used in cementitious mixture preparation. Ultrasonication enables exfoliation of the nanosheets of FG and RG, providing significant dispersion (as indicated by UV-Vis spectroscopy). These graphene-water suspensions were used to prepare the cementitious mixtures.

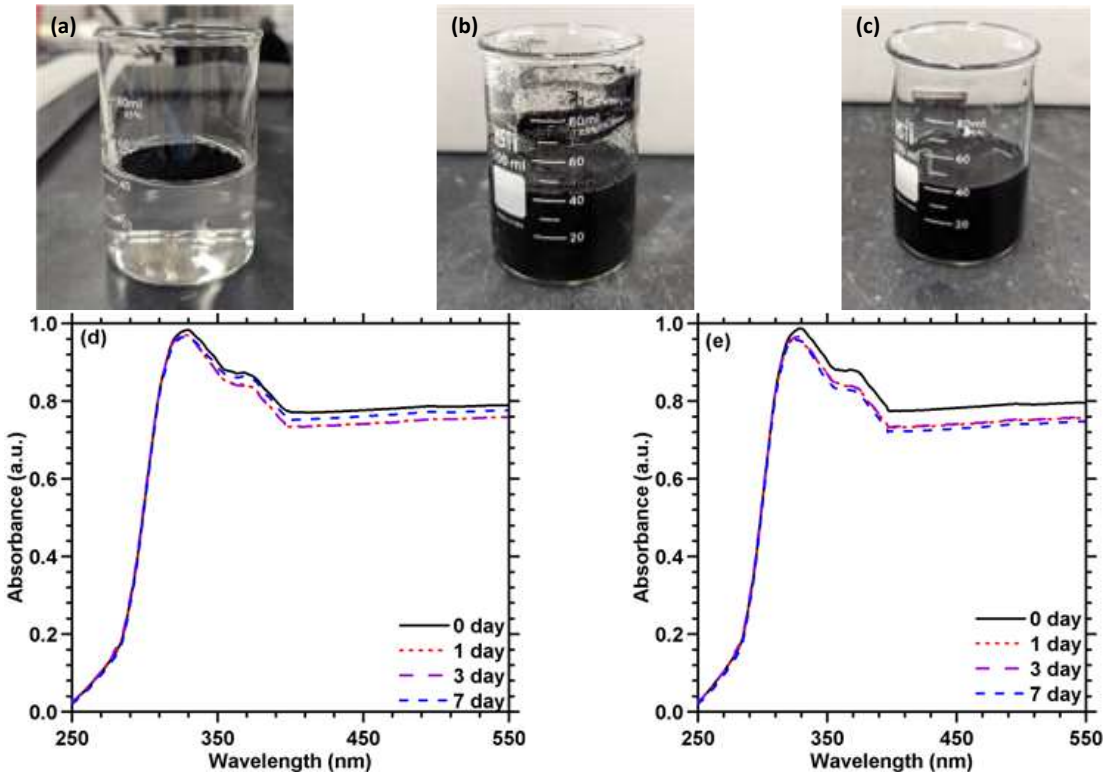

Figure 4: Graphene dispersion process: (a) addition of graphene in DI water; (b) after homogenization for 2 minutes, and (c) at the end of ultrasonication process (3 h). UV–Vis spectra of graphene dispersed solution at different ages for: (d) fractal graphene (FG), and (e) reactive graphene (RG). 0 d indicates measurement soon after completion of the dispersion procedure.

3.3 Test methods

To evaluate the influence of FG and RG in cement pastes, several tests were carried out. Since compressive strength is among the most important properties based on which cementitious mixtures are selected and specified, the strength of FG- and RG-modified mortars were determined in accordance with ASTM C 109 on 50 mm mortar cubes. Mortar cubes were prepared with a sand volume fraction of 50%. The cubes were stored in molds for 24 h in covered conditions, after which they were demolded and stored until the desired testing age (1-, 3-, 7-, 14-, and 28-d) in a moist environment (>95% RH) and a temperature of 23 ± 0.1 °C.

The use of ultrafine particles—graphene, in this case—changes the water demand and rheological characteristics of the concrete. In order to estimate these effects, ambient temperature (25 ± 0.1 °C) rheological experiments were carried out on pastes using TA instruments AR 2000EX rotational rheometer with a vane-in-cup geometry [47,48]. Approximately 40 mL of paste was placed in the rheometer geometry using a disposable syringe. The amount of time between the addition of mixing water and beginning the rheological experiment was approximately 5 min. A strain-controlled shear rate ramp study was conducted to evaluate the yield stress and plastic viscosity of the mixtures. Here, the shear rate was varied as follows: (i) a stepped ramp-up pre-shear phase from 10-to-100 s^{-1} lasting around 75 s to homogenize the paste, (ii) an immediate ramp-down to 0.005 s^{-1}, and (iii) a subsequent ramp-up phase from 0.005-to-100 s^{-1}, and a ramp down phase from 100-to-0.005 s^{-1}. Excluding the pre-shear phase, data was acquired every second until three consecutive torque measurements were within 8% of each other. The yield stress and plastic viscosity of the pastes were determined using the Bingham model (Eq.1).

$$\tau = \mu_p \dot{\gamma} + \tau_y \quad (1)$$

where τ = shear stress (Pa); μ_p = plastic viscosity (Pa.s); $\dot{\gamma}$ = shear rate (s^{-1}); τ_y = yield stress (Pa)

The heat evolution during hydration was determined using isothermal calorimetry (TAM Air micro calorimeter 2700 Series) at a constant temperature of 25 °C for 72 h. Approximately 15 g of paste was placed in a sealed sample vial immediately after mixing to minimize evaporation, and placed in the isothermal calorimeter. The extent of degree of hydration of pastes containing FG and RG were determined using thermo-gravimetric analysis (TGA) using a Perkin Elmer simultaneous thermal analyzer (STA 6000) at ages of 7-, and 28-d. Paste samples were cured under sealed conditions at a temperature of 23 ± 0.1 °C until the desired testing age. Tests were conducted in a N_2 environment at a gas flow rate of 20 $ml.s^{-1}$. The sample was heated to 50 °C and then held for 1 min, and then heated to 900 °C at a rate of 10 °C min^{-1}. The non-evaporable water contents (w_n) were determined as the difference in mass when the sample was heated from 105 °C to 900 °C, normalized by the mass at 900 °C, and corrected for the calcium carbonate content. Even though the test was not allowed to progress until 1000 °C, the mass loss at temperatures > 850 °C was noted to be insignificant, which is also reported elsewhere [49,50]. Calcium hydroxide (CH) contents at different ages were also determined based on the mass loss in the temperature range of decomposition of CH, taken as 400 °C – 530 °C.

The pore structure of the FG- and RG-modified pastes were determined using mercury intrusion porosimetry (MIP) [51,52] after 3-, 7-, and 28-d of hydration. A Quantachrome mercury intrusion porosimeter capable of exerting a maximum pressure of 414 MPa and evaluating a minimum pore diameter of 0.0036 μm was used. The test was performed in two stages - the low-pressure step evacuates the pores, fills them with mercury, and carries out pressurization to 414 kPa, while the high-pressure step reaches pressure up to 414 MPa. The applied pressure during the intrusion of mercury and pore diameter are related through the Washburn equation:

$$\Delta P = \frac{-4\,\sigma\cos\theta}{d} \quad (2)$$

where ΔP is the pressure required for mercury intrusion, *d* is the diameter of the pore being intruded, σ is the surface tension of mercury, and θ is the contact angle between mercury and pore wall. The contact angle and surface tension of mercury used were 130° and 0.485 Nm^{-1} respectively [51].

4. Structure and properties of FG- and RG-modified mixtures

4.1 Compressive strength

Prior research has shown substantial variability (of an order of magnitude) in the optimal dosages of graphene required to maximize the compressive strength of cementitious systems. This variability stems from the type of graphene and mixture proportions used. However, regardless of these variations, when graphene is added in amounts less than or exceeding the optimal dosage, there is a decline in strength (and, indeed, other properties) [7,40,53]. Since FG (and RG) has not been used in cementitious materials in the past, it is important to establish the changes in properties and performance of cementitious materials induced by these materials, given their differences with commonly used GO and rGO as explained earlier. Therefore, 1-, 3-, and 7-d compressive strengths of cement mortars containing up to 0.10% (by mass of cement) FG were determined as shown in Figure 5. It can be seen that the compressive strengths of all FG-containing mortars are higher than that of the plain OPC mortar at all ages. The strength enhancement at very early ages (especially at 1-, and 3-d) is more prominent. Among all the mixtures, FG-0.02 (i.e., containing 0.02% of FG) had the highest strength at 7-d. Beyond a FG dosage of 0.04%, the 7-d strength declines and remains more-or-less constant regardless of the graphene dosage. Hence the maximum graphene dosage for all further studies were limited to 0.04% by mass of cement.

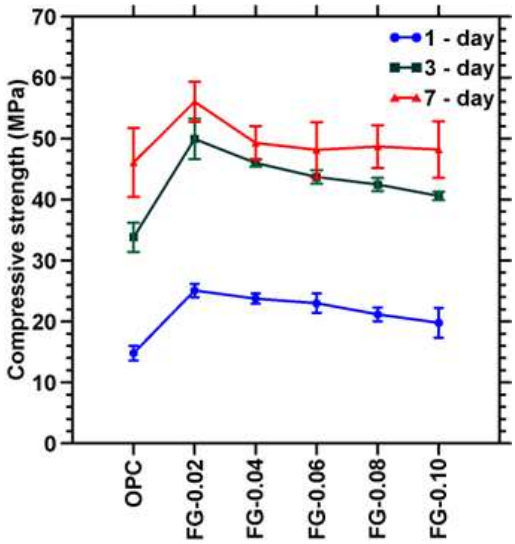

Figure 5: Early-age strength development as a function of FG dosage. The numbers next to FG indicate the FG dosage as a % by mass of cement.

Compressive strengths until 28-d for mortars containing up to 0.04% (by mass of cement) of FG and RG are shown in Figures 6(a) and (b). It is found that small dosages of FG or RG enhances the compressive strength at all ages, with more pronounced enhancements at early ages. This aspect could be exploited in concretes featuring high volume replacement of cement by less-reactive materials; wherein a small dosage of graphene would compensate for the strength loss at early ages. The increase in the compressive strengths of the graphene-modified mixtures can be attributed to the

seeding effects of ultrafine graphene platelets that accelerate cement hydration [21,54–56]. This results in small amounts of graphene being able to reduce the porosity and improving solid-phase connectivity, thereby increasing the strength. These phenomena will be elucidated in detail in the following sections. Another mechanism that is reported to improve the strength is the enhancement in interfacial bonding and mechanical interlocking with the cementitious matrix facilitated by the graphene particles, which positively affects load-transfer efficiency and reduces stress concentration [57]. It is likely that the graphene nanoparticles occupy the interfacial transition zone (ITZ) in cement mortars, and thus the enhanced formation of hydrates on and around graphene serves to both densify and mechanically strengthen the ITZ. The 28-d compressive strength is highest for the FG-0.04 mixture while for RG, the 28-d strength is found to be the highest for the RG-0.02 mixture. Pristine graphene such as FG reinforces the matrix through adhesion and friction between graphene sheets and the hydration products [58], and up to a dosage of 0.04% (the maximum investigated in this work) [59–61], it is dispersed rather efficiently in the cementitious matrix. In the case of RG-modified mixtures, the oxygen atoms in the COOH groups of RG act as water adsorption sites, and hence, beyond a certain dosage of RG (in this case, 0.02%), agglomeration occurs more easily. Since water is adsorbed by the functional groups in RG, they could also influence the rate of hydration [62]. Results on hydration and pore structure discussed later also lend credence to this observation.

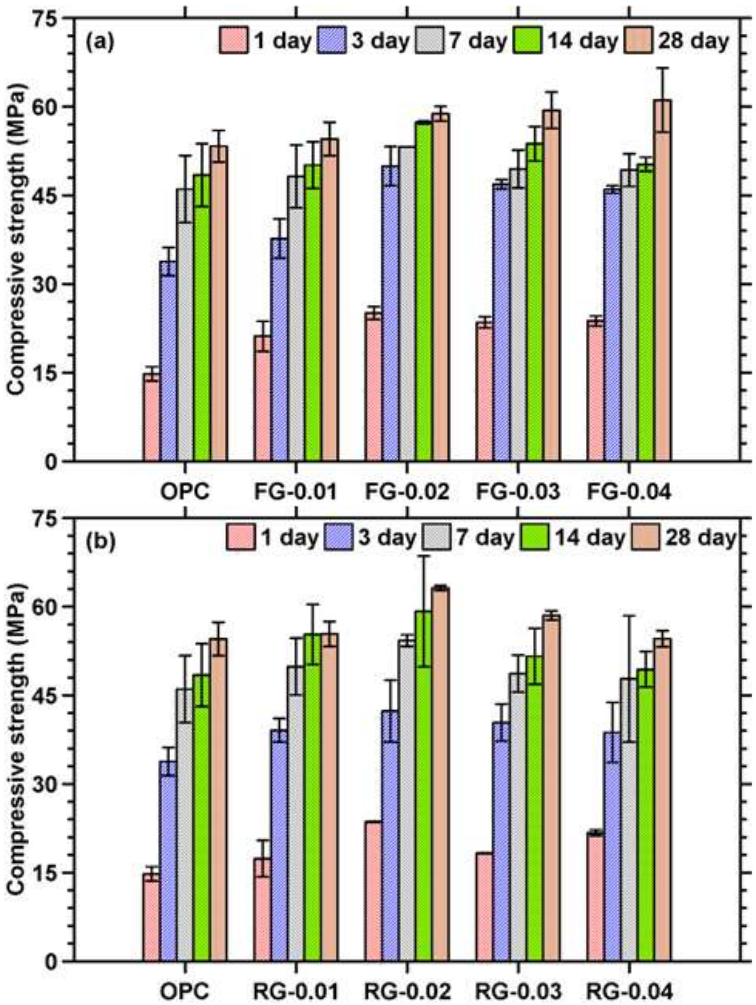

Figure 6: Compressive strengths of: (a) FG-modified mortars, and (b) RG-modified mortars until an age of 28-d. The numbers next to FG and RG indicate the fractal or reactive graphene dosage as a % by mass of cement.

Figures 7(a) and 7(b) depict the percentage increase in compressive strength of FG- and RG-modified mortars, respectively, when compared to the control mortar. It is clear that the graphene-modified mixtures show significant strength enhancement at early ages (especially 1-, and 3-d). The FG-modified mixtures show ~40-70% and 10-50% higher strength compared to the control mortar at 1-, and 3-d, respectively; the corresponding increases for RG-modified mixtures are ~20-60% and 10-25%, respectively. Recent publications have highlighted notable disparities in the optimal dosages of GO/rGO and GNPs dosages for enhancing the mechanical properties of cement-based systems [7,14,40,63]. In general, GO-modified mixtures (with comparable w/c as used here) showed an increase of ~20-40% at early ages (at 3-, and 7-d) at various GO contents (0.02–0.30% by mass of cement) [64–66]; while GNP-modified mixtures showed strength improvement of 30-60% after 28-d at significantly higher dosages of ~0.40-0.80% by mass of cement [2,64,67,68]. rGO-modified mixtures are reported to show 10-15% increase in compressive strength compared to control mortar mixtures at dosages of 0.02-0.06% by mass of cement (similar to the dosages used in this study) [18]. This shows that FG and RG can be used in dosages similar to or less than those used in other studies with GNPs, GO, or rGO to obtain comparable strength enhancements. The cost impact of such dosage reduction is significant, and considering: (a) carbon- and energy-efficient manufacturing processes of FG and RG (see Section 5 for more details), and (b) the ability to reduce ~15% of cement for the same strength as the control mixture, this enables cost-efficient production of low carbon concretes with superior properties.

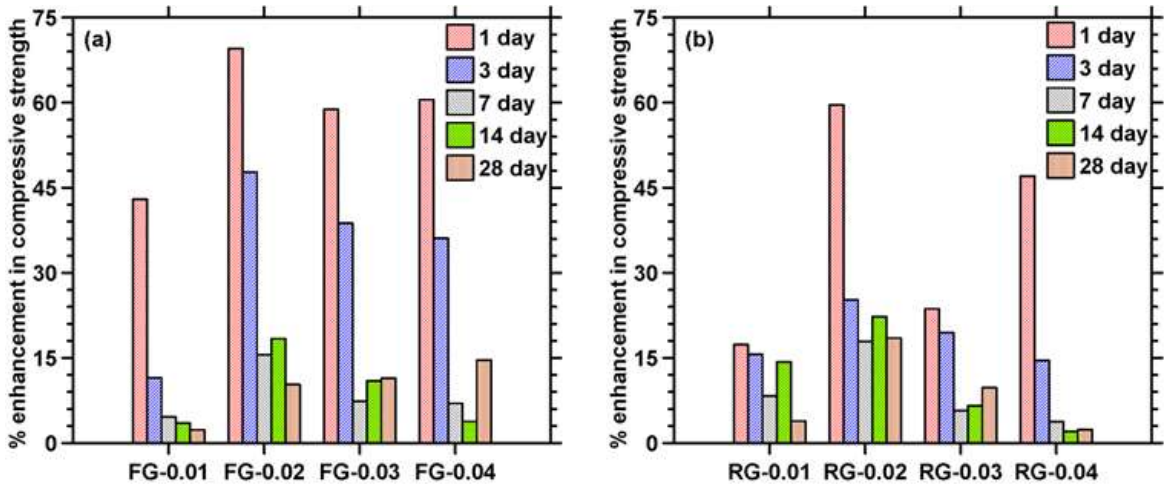

Figure 7: Strength enhancements compared to control mortar for: (a) FG-modified mortars, and (b) RG-modified mortars at all ages studied.

4.2. Rheological parameters: Yield stress and plastic viscosity

Yield stress and plastic viscosity are important rheological metrics for cementitious systems. Yield stress (τ_y), which is attributed to particle-scale properties and packing, is generally defined as the non-zero (finite) stress at zero strain rate (based on Bingham model). The plastic viscosity (μ_p) of particulate suspensions is considered to be primarily influenced by inter-particle friction and surface contacts, wherein decreasing the inter-particle (friction) forces by increasing the particle spacing (or by decreasing surface contacts) results in a decrease in plastic viscosity. Figure 8 presents the yield stress and plastic viscosity of the control, FG-modified, and RG-modified pastes. The graphene-modified pastes exhibit significantly higher yield stress and plastic viscosity as compared to the control paste. The yield stress of graphene-modified pastes is about 2 to 2.5 times higher than that of the control paste; making the use of small dosages of graphene an attractive strategy to proportion mixtures for applications such as concrete 3D printing, where higher yield stresses are desirable to ensure extrudability and shape stability [69,70]. The significant increase in yield stress is attributed to: (a)

enhanced particle packing (jamming effects) with increase in graphene dosage , and (b) higher specific surface area of graphene nanoparticles that makes movement of water for the lubrication of cement particles harder [71–73]. The slight reduction in yield stress of both the FG- and RG-modified pastes at a higher dosage (0.04 wt%) likely reflects the agglomeration of graphene particles above the optimum dosage. It is also noticed that the RG-modified pastes exhibit ~5-15% higher yield stress than the FG-modified pastes, which is likely attributable to the presence of -COOH functional groups in RG. The negatively charged RG interacts electrostatically with positively charged cement particles, leading to the formation of floccules and agglomerates that trap more free water [71,72].

Although the plastic viscosities of graphene-modified pastes are higher than that of the control paste (due to large specific surface area of graphene and reduction in water mobility), the change in plastic viscosity is not as significant as that in yield stress. This suggests that the effects of graphene inclusion are less significant in suspension once flow has been initiated. Plastic viscosity is acknowledged to be more strongly influenced by the nature of the fluid and the solid fraction and size distribution of the suspended particles [74,75]. As the particle size distribution and solid loading are more-or-less equivalent in the pastes evaluated here, plastic viscosity is not significantly influenced by the considered dosages of graphene.

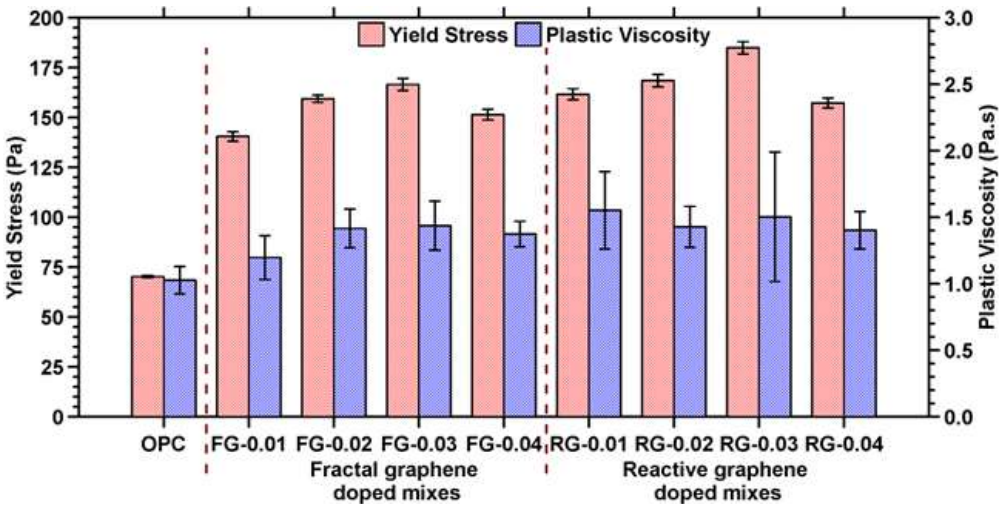

Figure 8: Yield stress and plastic viscosity values of FG- and RG-modified pastes.

4.3. Hydration and product formation

4.3.1. Hydration heat release using isothermal calorimetry

Early age hydration kinetics of FG- and RG-modified pastes were determined using isothermal calorimetry at a temperature of 25 °C as described earlier. The heat flow curves until a hydration time of 36 h are shown in Figures 9(a) and (b). As can be seen, the acceleration peaks (i.e., the main hydration peaks) are higher for all the graphene-modified mixtures (both FG and RG) when compared to that of the plain OPC paste. Cumulative heat released at the end of 72 h was in the range of 205 – 220 J/g of binder for the FG- and RG-modified pastes (as compared to 180 J/g for the plain OPC paste). These observations suggest that the high surface area FG and RG particles act as hydration-enhancing filler materials by providing additional sites for C-S-H nucleation [76,77]. Zeta potential measurements have shown that Ca^{2+} particles released from cement are adsorbed on graphene surfaces, thereby developing ionic clusters that enhance the formation of C-S-H [78].

A comparison of the heat flow curves of FG- and RG-modified pastes shows more intense acceleration peaks for the RG-modified cement pastes at all graphene dosages. Moreover, while the incorporation of FG does not alter the time of occurrence of the acceleration peak, the use of RG shifts the acceleration peaks slightly to earlier times. The negatively charged functional groups in RG have more affinity to Ca^{2+} ions, which increases the ionic mobility and enhances cement hydration, thus explaining both the aforementioned observations. Furthermore, the functional groups also reduce the Van der Waal's forces between the sheets and make them more hydrophilic, which in turn enhances the reactivity of cement particles in suspension. Figure 9(b) shows that the magnitude of the acceleration peak is the highest for the RG-0.02 paste; in other words, a dosage of RG higher than 0.02% detrimentally affects hydration (though the heat flow rate still exceeds that of the control OPC paste). This can be explained based on increased surface energy in the presence of functional groups, which could hinder dispersion in aqueous solutions—even though the functional groups have more affinity to Ca^{2+}, beyond a certain dosage, they are agglomerated, thereby causing less efficient dispersion. This phenomenon is also noticed in the compressive strength results, where maximum strength enhancement (with respect to the control mixture) is observed for the RG-0.02 mixture. The hydration heat measurements thus corroborate the selection of optimal dosages of FG- and RG-modified mixtures.

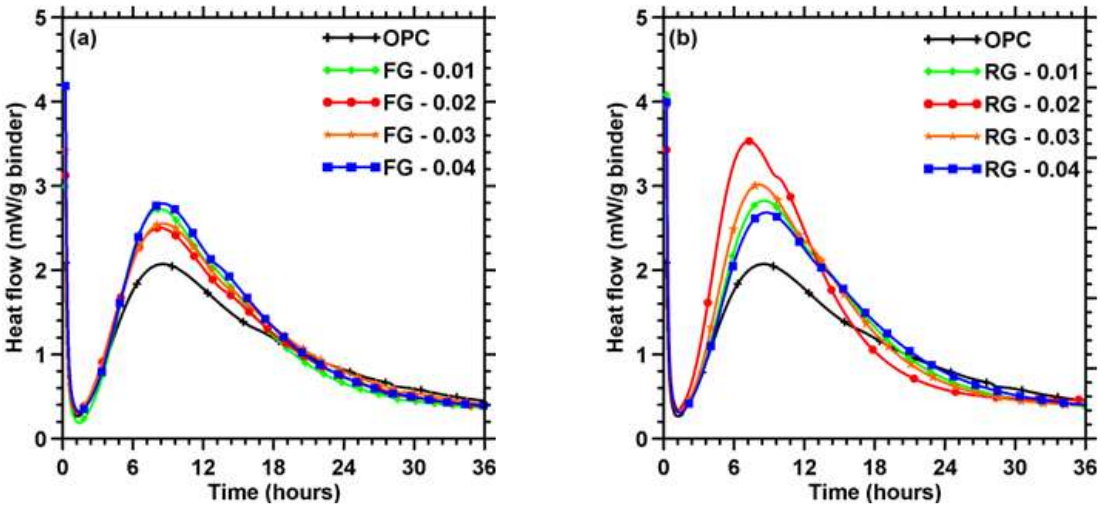

Figure 9: Heat flow curves of (a) FG-modified pastes, and (b) RG-modified pastes.

4.3.2. Product formation

Thermogravimetric analysis (TGA) was carried out to quantify the reaction products in the plain and graphene-modified pastes. Representative differential thermogravimetric (DTG) curves are shown in Figures 10(a) and (b). The DTG curves show several distinguishable peaks attributable to the decomposition of: (i) C-S-H and ettringite around 120-130 °C, and (ii) calcium hydroxide (CH) around 400-530 °C. To elucidate the role of graphene in hydration product formation, the evolution of non-evaporable water contents (w_n) and CH contents at 7- and 28-d of hydration were determined; the results are shown in Figures 11(a) and (b). An increase in w_n and CH contents with time is noticeable between 7-, and 28-d. The graphene-modified pastes show higher w_n and CH contents than the control paste at all graphene dosages and ages, indicating the influence of FG and RG as nanoscale fillers in enhancing cement reactivity and the formation of hydration products, which has been demonstrated earlier using isothermal calorimetry. The w_n contents follow a general trend similar to that of compressive strength development of FG- and RG-modified mixtures. Both w_n and CH contents decrease beyond a dosage of 0.02% by mass of cement for both FG-, and RG-modified mixtures at 7-d; these patterns mirror the trend noted in strength evolution (Figure 6). For the RG-modified pastes,

the w_n and CH contents decrease beyond a dosage of 0.02% at 28-d; this is hypothesized to result from the reaction between the carboxylate functional groups and Ca^{2+}. The product adsorbs water molecules, thereby affecting cement hydration [40,79]. When the peak values of w_n and CH are considered for both the FG- and RG-modified pastes, it is seen that at the optimal dosages (0.04% for FG and 0.02% for RG – as indicated by the compressive strength and heat of hydration results), w_n and CH contents are comparable or higher for the RG-modified mixture, even at a lower dosage, demonstrating the efficiency of functionalization. The increased amounts of hydration products result in overall improvement in properties, including a reduction in porosity and pore size, as is elucidated in the following section.

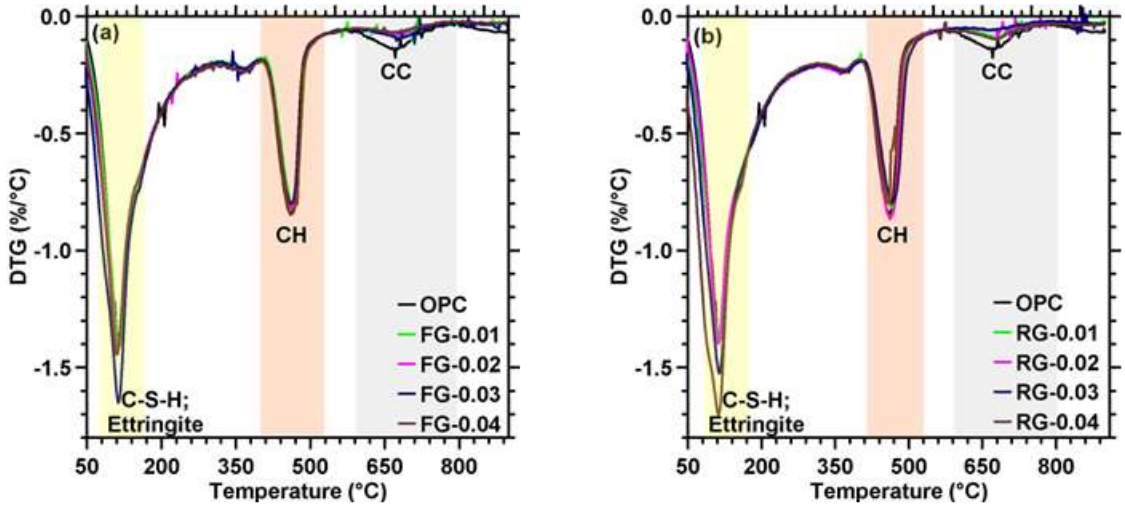

Figure 10: Representative 28-d DTG profiles of: (a) FG-modified, and (b) RG-modified pastes.

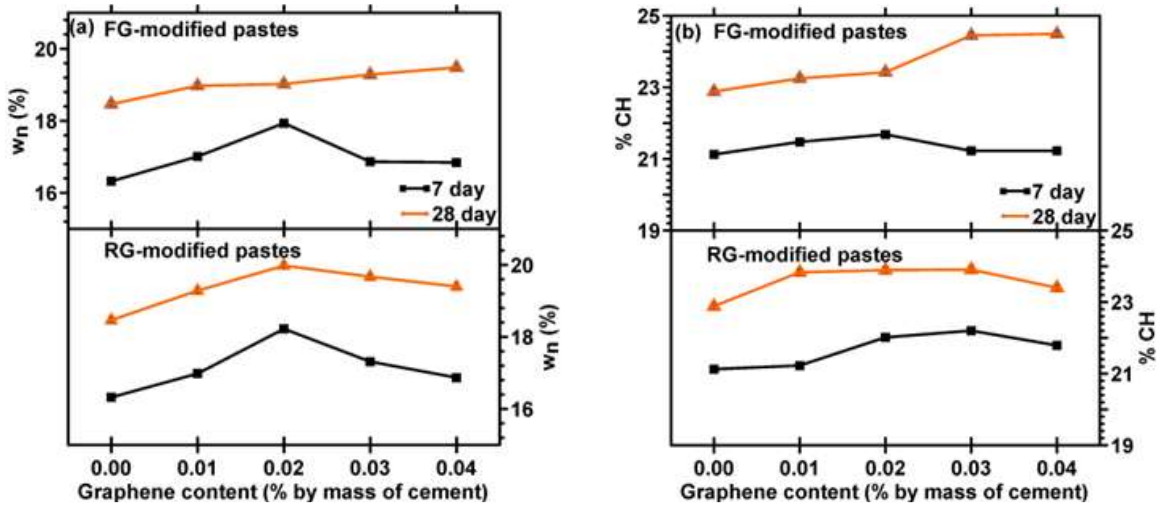

Figure 11: (a) w_n, and (b) CH contents of FG-, and RG-modified pastes at 7-d and 28-d of hydration.

4.4. Pore structure from mercury porosimetry

The major pore structure features that are influential in the performance of cementitious materials (porosity and critical pore size) are reported in this section for FG- and RG-modified pastes at early and later ages of hydration. While the determination of pore size distribution using MIP has been shown to be inaccurate due to ink-bottle and other effects [52,80], it is well accepted that the total volume of mercury intruded (from which porosity can be deduced) and the critical or the percolating pore size obtained from MIP are reliable indicators of concrete durability. Figure 12(a) shows the porosities of

all pastes at different ages of curing, determined using the intrusion portion of the MIP data. The porosities of the FG- and RG-modified pastes are lower than that of the control OPC paste at all ages. The porosity reduction at early ages is more pronounced than at later ages, in line with the compressive strength results. At 3-d, porosity reduction between 10-20% for FG-modified pastes and 30-60% for RG-modified pastes are noted; while at 28 days, the porosity reduction ranges between 10-30% and 20-40%, respectively. This can be attributed to the reasons that have been explained in the previous sections. At all ages, and for all dosages considered, the RG-modified pastes have lower porosities than their FG-modified counterparts. The porosity reduction also mirrors the trends in strength development described in section 4.1.

The critical pore size or the threshold pore size is the maximum pore diameter (D) in the D – dV/dlogD relationships obtained from MIP data. The critical pore diameter has been related to the durability of concrete, since it indicates the threshold pore size for percolation. Figure 12(b) shows the critical pore diameter of all the FG- and PG-modified pastes. The effect of FG and RG on pore structure refinement is evident from this figure. The critical pore size reduction is much more exaggerated compared to the porosity reduction, for both types of graphene, especially at early ages. Once again, the explanation for this observation lies in the modification of cement hydration effected by FG and RG, as described in the foregoing sections. RG is up to 25% more efficient in pore size reduction, depending on the curing age. The optimal values of FG and RG for lower porosities and pore sizes are also in conformance with those for heats of hydration, product formation, and compressive strength.

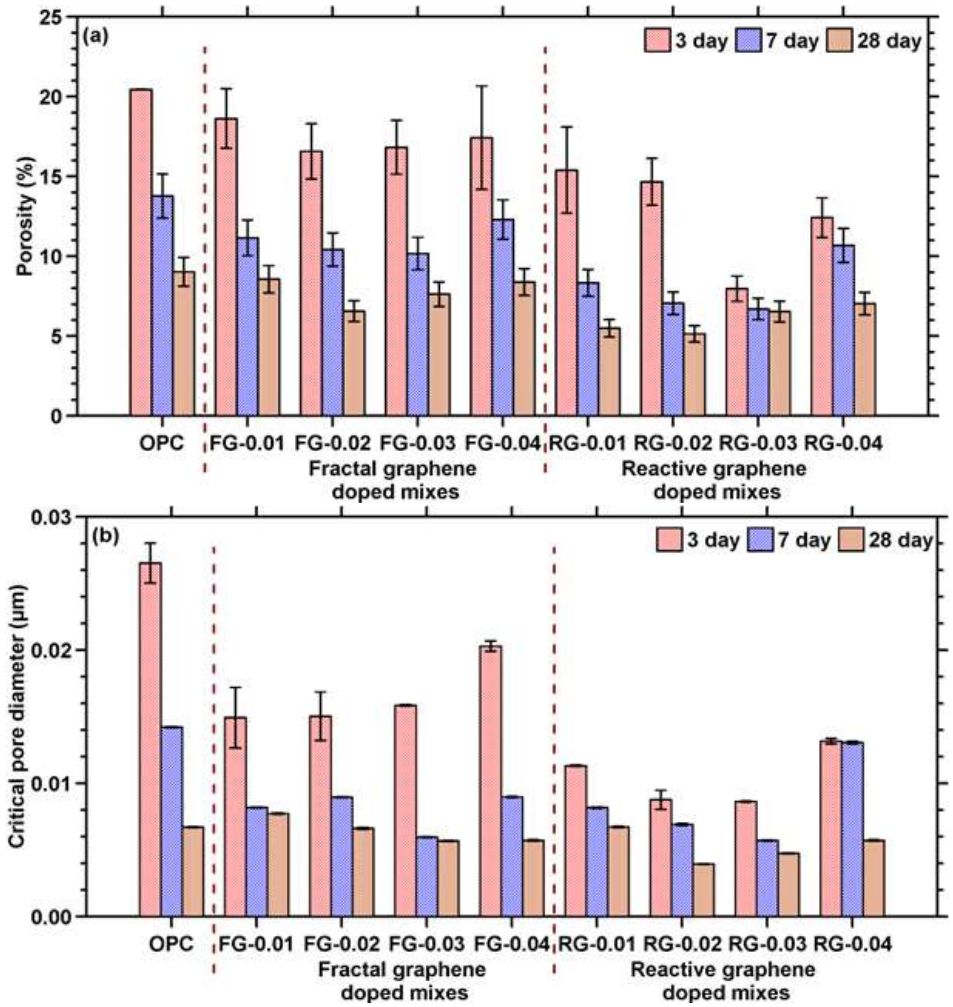

Figure 12: (a) Porosities, and (b) critical pore sizes of FG- and RG-modified cement pastes after 3-, 7-, and 28-d of hydration.

5. Life cycle analysis of cementitious binders containing FG and RG

The use of graphene has been shown to beneficially impact the properties of cement-based materials; however, logistical and economic obstacles in scaling up graphene production, and energy and environmental impacts [40,63], still remain an impediment to its widespread use. The high-yield, scalable detonation synthesis method is expected to be a solution to some of these issues. To quantify the impacts of this process, and to establish its beneficial attributes, published literature [27,31,81] was used to determine the energy demand and CO_2 impact (global warming potential, GWP) of 1 kg of GNP/GO produced using four different, well-established methods, in addition to detonation synthesis; the results are shown in Figures 13(a) and (b). While detonation synthesis produces FG (similar to traditional GNP, albeit with smaller sizes), a combination of Fenton oxidation with detonation synthesis, which is used to produce RG, is considered here. The energy and environmental impact of detonation synthesis for FG production was obtained from literature [30]. The use of Fenton oxidation produces 1.33 g of functionalized graphene from 1 g of graphene, through the use of 0.1 M $FeSO_4 \cdot 7H_2O$ aqueous solution, 98% H_2SO_4, 30% H_2O_2, and HCl/H_2O_2, as described elsewhere [36]. The energy and environmental impacts of this production process was calculated using available information from openLCA [82]. Commercial functionalized graphene (or GO) is produced using Hummer's method [81], and hence it is used for comparison with RG. Other methods considered here for comparison are chemical vapor deposition (CVD), biomass-based flash Joule heating (FJH), and ultrasonic exfoliation, which are commonly used approaches and for which energy-and-emissions impact data are readily available [27,31]. As can be noticed from Figures 13(a) and (b), CVD, Hummer's method, and exfoliation have significantly higher energy-and-emissions impact than detonation synthesis. Biomass-based FJH has lower emissions than many other processes because of the use of carbon-rich biomass wastes [27]. Overall, Figures 13(a) and (b) show that the detonation synthesis method has a significantly lower energy demand and GWP because of the highly exothermic reaction and the very low input energy to initiate the reaction (even without considering the utility value of syngas that is produced). This information is used in the comparative LCA of FG- and RG-modified mortars as described below.

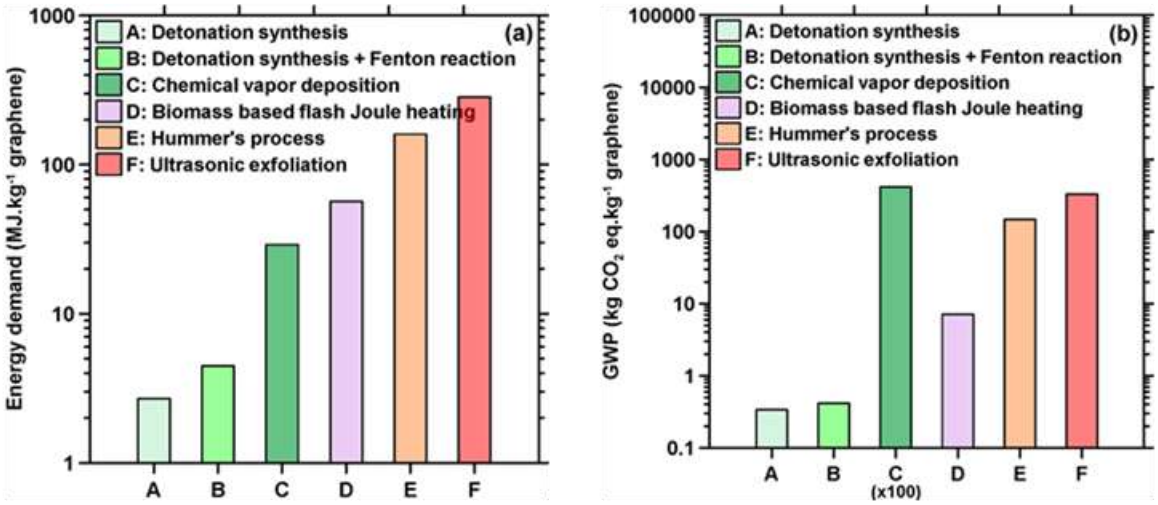

Figure 13: (a) Energy demand, and (b) GWP of different graphene production processes, showing the high energy- efficiency and environmental benefits of detonation synthesis [27,30,31,36,81].

The goal and scope of the comparative LCA effort is to evaluate the carbon footprint and energy demand of the mortar mixtures proportioned with small amounts of FG or RG as an additive, given the energy-and-emissions impact associated with graphene production as shown above. In the absence of data pertinent to serviceability and end-of-life phases of graphene-modified mixtures, this LCA follows a cradle-to-gate approach, which includes the stages of raw material production, material transportation, and mortar mixing. The functional unit used is 1 m^3 of mortar. The analysis is limited to mortar mixtures containing plain OPC, and 0.02% and 0.04% FG or RG by mass of cement. More details on LCA parameters for 1 m^3 of concrete or mortar can be found in the supplementary information (SI) as well as in other published literature [83].

For the impact assessment phase, Tool for the Reduction and Assessment of Chemical and other Environmental Impacts (TRACI; version 2.1) is used [84]. Among the environmental impact categories provided by TRACI 2.1, only the energy demand and global warming potential (GWP) are used here. Since RG is produced from FG made using detonation synthesis, the energy demand and GWP for RG were evaluated using openLCA as mentioned earlier by creating a process flow based on Fenton reaction [36]. The dispersion of FG and RG in water necessitates additional energy and creates emissions, which was calculated based on the power and capacity of industrial-scale homogenizer and ultrasonicator that can handle ~350 kg of liquid, and incorporated into the LCA.

The energy demand and GWP for 1 m^3 of plain OPC mortar was determined to be 4608.6 MJ and 809.8 kg CO_2-eq respectively, from the analysis. Note that the higher value of GWP is because of the higher cement content in the mortar (in typical OPC concretes, this value is ~400 kg CO_2-eq per m^3 of concrete). The FG- and RG-modified mixtures showed only minimal increases in energy demand and GWP (~1.0-1.5%) because: (a) the dosages of FG and RG are very small – in a m^3 of mortar, there is only 320 g of FG or RG at the highest dosage levels, compared to ~800 kg of OPC; and (b) the impacts of FG and RG production are lower as shown in Figure 13. Most of the slightly increased energy demand and GWP is due to the electricity requirement for dispersion. To better elucidate the advantages of incorporating FG and RG in mortar mixtures, energy demand and GWP were normalized with the 28-d compressive strengths of the respective mixtures, and are shown in Figures 14(a) and (b). Because of their higher 28-d strengths, the RG-0.02 mixture shows approximately 15% reduction in both the energy demand and GWP. If it is required that the graphene-modified mixtures demonstrate the same strength as the control OPC mixture, then the cement content can be reduced, which also could result in similar or better impacts. Note that 0.02% by mass of cement was arrived at as the optimal dosage for RG based on strength and other parameters. For the optimal FG dosage (0.04% by mass of cement), the normalized carbon footprint and energy demand are comparable to that of the RG-0.02 mixture. Even though more FG is used in this mixture as compared to the optimal RG-modified mixture, the energy and carbon impacts of its production are lower as compared to RG, resulting in such an outcome. The LCA described here shows that FG and RG can be appropriately chosen to optimize both the performance and impact categories. A 15% reduction in the chosen impact categories, which is typically obtained with a 15-20% replacement of cement with fly ash, can be achieved through the use of small amounts FG or RG, but with the beneficial attribute of not compromising the early-age strengths (in fact, with a potential to significantly enhance early-age strengths).

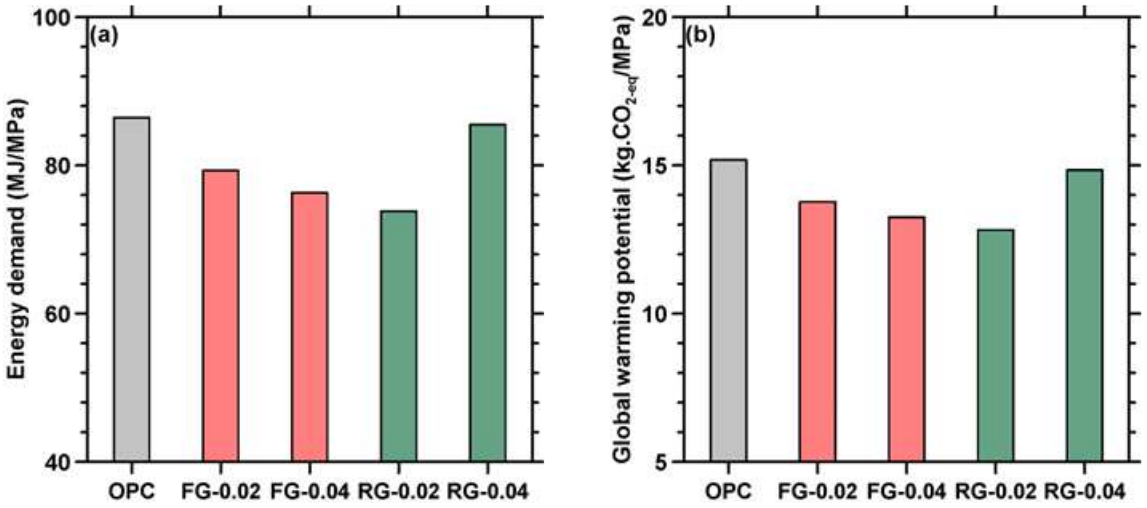

Figure 14: (a) Energy demand, and (b) Global Warming Potential for 1 m^3 of mortar normalized with the 28-d compressive strengths.

6. Summary and conclusions

This paper focuses on the use of graphenes—produced using a novel, scalable, and cost-effective detonation synthesis method—in cement-based mixtures. Two graphene types—fractal graphene (FG) and reactive graphene (RG), the latter produced from FG using a functionalization method—are evaluated at dosages ≤0.04% by mass of cement. FG and RG have lateral dimensions of 20-50 nm, and a z-axis dimension of <5 nm. The graphene production method, salient differences between conventional methods of producing graphene, and the characteristics of the product, which are consistent with existing norms, have been described in detail. Aqueous solutions containing FG and RG were prepared using a homogenization and ultrasonication method, and the particles were found to be well dispersed even after an extended rest period. The following conclusions are deduced from the studies on FG and RG in cementitious mixtures:

(i) Both FG and RG resulted in significant enhancements of up to 70% in the early-age (1- and 3-d) compressive strengths of mortars. The 28-d strengths were found to be the highest for the RG-0.02 and FG-0.04 mixtures, with an enhancement of ~15% compared to the control mixture. The dosages for FG and RG needed for similar strength enhancements are generally similar to or lower than those for conventionally used GNP/GO.

(ii) The yield stress of fresh suspensions containing up to 0.04% of FG or RG more than doubled as compared to the control OPC paste; thus enabling small dosages of graphene to be used in applications such as concrete 3D printing. Though the plastic viscosities also increased with graphene addition, the changes were not as significant as those for yield stress.

(iii) Both FG and RG resulted in acceleration of cement hydration kinetics. RG was found to be more influential than FG at smaller dosages, increasing the magnitude of the acceleration peak as well as shifting it to slightly earlier times. A smaller dosage of RG—compared to FG—was more effective in enhancing hydration kinetics; this is due to the presence of functional groups with more affinity to Ca^{2+} ions, which increases the ionic mobility and enhances hydration. The reaction product formation, quantified through measurements of non-evaporable water contents and CH contents, were also found to be in line with the hydration kinetics results.

(iv) Small amounts of FG and RG have a significant influence on the pore structure of pastes at all ages. Both total porosity and critical pore size were reduced, with the effect being more pronounced at

early ages. The RG-modified pastes showed greater reduction in porosity and improved refinement of pore sizes. The critical pore size reduction was more pronounced than porosity reduction, pointing to the potential of small amounts of graphene to beneficially impact concrete durability (given that moisture and ionic transport is more influenced by pore size refinement than porosity reduction).

(v) A cradle-to-gate LCA demonstrated the benefits in energy demand and GWP when FG or RG is incorporated into cementitious mortars. Both the FG-0.04 and RG-0.02 mixtures (based on the optimal dosages of FG and RG for properties) showed 10-15% reduction in the energy demand and GWP normalized by the compressive strength.

In summary, this work has shown that FG and RG manufactured through a cost-, energy-, and CO_2-efficient, scalable detonation synthesis procedure can beneficially impact the engineering and environmental performance of concretes. Long-term performance studies of FG- and RG-containing mixtures are necessary to establish their true potential but given the improved pore structure features and hydration products as determined in this study, better durability as compared to control mixtures can be justifiably expected.

7. Acknowledgments

The authors sincerely acknowledge partial support from National Science Foundation (NSF) through Grant No. OISE 2020095 towards the conduct of this project. HydroGraph produced and supplied the different types of graphene for this work. The cement used in this work was supplied by Salt River Materials Group (Phoenix Cement). We acknowledge the use of experimental facilities within the Center for Carbon-Efficient and Advanced Manufacturing of Materials and Structures (CAMMS) at Arizona State University.

8. References

(1) Wang, M.; Wang, R.; Yao, H.; Farhan, S.; Zheng, S.; Du, C. Study on the Three Dimensional Mechanism of Graphene Oxide Nanosheets Modified Cement. *Construction and Building Materials* **2016**, *126*, 730–739. https://doi.org/10.1016/j.conbuildmat.2016.09.092.

(2) Lv, S.; Ma, Y.; Qiu, C.; Sun, T.; Liu, J.; Zhou, Q. Effect of Graphene Oxide Nanosheets of Microstructure and Mechanical Properties of Cement Composites. *Construction and Building Materials* **2013**, *49*, 121–127. https://doi.org/10.1016/j.conbuildmat.2013.08.022.

(3) Gong, K.; Pan, Z.; Korayem, A. H.; Qiu, L.; Li, D.; Collins, F.; Wang, C. M.; Duan, W. H. Reinforcing Effects of Graphene Oxide on Portland Cement Paste. *Journal of Materials in Civil Engineering* **2015**, *27* (2), A4014010. https://doi.org/10.1061/(ASCE)MT.1943-5533.0001125.

(4) Lv, S.; Liu, J.; Sun, T.; Ma, Y.; Zhou, Q. Effect of GO Nanosheets on Shapes of Cement Hydration Crystals and Their Formation Process. *Construction and Building Materials* **2014**, *64*, 231–239. https://doi.org/10.1016/j.conbuildmat.2014.04.061.

(5) An, J.; McInnis, M.; Chung, W.; Nam, B. H. Feasibility of Using Graphene Oxide Nanoflake (GONF) as Additive of Cement Composite. *Applied Sciences* **2018**, *8* (3), 419. https://doi.org/10.3390/app8030419.

(6) Mohammed, A.; Al-Saadi, N. T. K.; Al-Mahaidi, R. Utilization of Graphene Oxide to Synthesize High-Strength Cement-Based Adhesive. *Journal of Materials in Civil Engineering* **2017**, *29* (4), 04016258. https://doi.org/10.1061/(ASCE)MT.1943-5533.0001705.

(7) Zhang, P.; Wang, M.; Han, X.; Zheng, Y. A Review on Properties of Cement-Based Composites Doped with Graphene. *Journal of Building Engineering* **2023**, 106367. https://doi.org/10.1016/j.jobe.2023.106367.

(8) Zhu, Y.; Murali, S.; Cai, W.; Li, X.; Suk, J. W.; Potts, J. R.; Ruoff, R. S. Graphene and Graphene Oxide: Synthesis, Properties, and Applications. *Advanced Materials* **2010**, *22* (35), 3906–3924. https://doi.org/10.1002/adma.201001068.

(9) Liu, C.; Huang, X.; Wu, Y.-Y.; Deng, X.; Zheng, Z.; Xu, Z.; Hui, D. Advance on the Dispersion Treatment of Graphene Oxide and the Graphene Oxide Modified Cement-Based Materials. *Nanotechnology Reviews* **2021**, *10* (1), 34–49. https://doi.org/10.1515/ntrev-2021-0003.

(10) Liu, C.; Chen, F.; Wu, Y.; Zheng, Z.; Yang, J.; Yang, B.; Yang, J.; Hui, D.; Luo, Y. Research Progress on Individual Effect of Graphene Oxide in Cement-Based Materials and Its Synergistic Effect with Other Nanomaterials. *Nanotechnology Reviews* **2021**, *10* (1), 1208–1235. https://doi.org/10.1515/ntrev-2021-0080.

(11) Zhao, Z.; Qi, T.; Zhou, W.; Hui, D.; Xiao, C.; Qi, J.; Zheng, Z.; Zhao, Z. A Review on the Properties, Reinforcing Effects, and Commercialization of Nanomaterials for Cement-Based Materials. *Nanotechnology Reviews* **2020**, *9* (1), 303–322. https://doi.org/10.1515/ntrev-2020-0023.

(12) Asim, N.; Badiei, M.; Samsudin, N. A.; Mohammad, M.; Razali, H.; Soltani, S.; Amin, N. Application of Graphene-Based Materials in Developing Sustainable Infrastructure: An Overview. *Composites Part B: Engineering* **2022**, *245*, 110188. https://doi.org/10.1016/j.compositesb.2022.110188.

(13) Mu, S.; Yue, J.; Wang, Y.; Feng, C. Electrical, Piezoresistive and Electromagnetic Properties of Graphene Reinforced Cement Composites: A Review. *Nanomaterials* **2021**, *11* (12), 3220. https://doi.org/10.3390/nano11123220.

(14) Zhao, L.; Guo, X.; Song, L.; Song, Y.; Dai, G.; Liu, J. An Intensive Review on the Role of Graphene Oxide in Cement-Based Materials. *Construction and Building Materials* **2020**, *241*, 117939. https://doi.org/10.1016/j.conbuildmat.2019.117939.

(15) Du, H.; Pang, S. D. Enhancement of Barrier Properties of Cement Mortar with Graphene Nanoplatelet. *Cement and Concrete Research* **2015**, *76*, 10–19. https://doi.org/10.1016/j.cemconres.2015.05.007.

(16) Mokhtar, M. M.; Abo-El-Enein, S. A.; Hassaan, M. Y.; Morsy, M. S.; Khalil, M. H. Mechanical Performance, Pore Structure and Micro-Structural Characteristics of Graphene Oxide Nano Platelets Reinforced Cement. *Construction and Building Materials* **2017**, *138*, 333–339. https://doi.org/10.1016/j.conbuildmat.2017.02.021.

(17) Sun, S.; Ding, S.; Han, B.; Dong, S.; Yu, X.; Zhou, D.; Ou, J. Multi-Layer Graphene-Engineered Cementitious Composites with Multifunctionality/Intelligence. *Composites Part B: Engineering* **2017**, *129*, 221–232. https://doi.org/10.1016/j.compositesb.2017.07.063.

(18) Qureshi, T. S.; Panesar, D. K. Impact of Graphene Oxide and Highly Reduced Graphene Oxide on Cement Based Composites. *Construction and Building Materials* **2019**, *206*, 71–83. https://doi.org/10.1016/j.conbuildmat.2019.01.176.

(19) Tong, T.; Fan, Z.; Liu, Q.; Wang, S.; Tan, S.; Yu, Q. Investigation of the Effects of Graphene and Graphene Oxide Nanoplatelets on the Micro- and Macro-Properties of Cementitious Materials.

Construction and Building Materials **2016**, *106*, 102–114. https://doi.org/10.1016/j.conbuildmat.2015.12.092.

(20) Li, X.; Wang, L.; Liu, Y.; Li, W.; Dong, B.; Duan, W. H. Dispersion of Graphene Oxide Agglomerates in Cement Paste and Its Effects on Electrical Resistivity and Flexural Strength. *Cement and Concrete Composites* **2018**, *92*, 145–154. https://doi.org/10.1016/j.cemconcomp.2018.06.008.

(21) Li, W.; Li, X.; Chen, S. J.; Long, G.; Liu, Y. M.; Duan, W. H. Effects of Nanoalumina and Graphene Oxide on Early-Age Hydration and Mechanical Properties of Cement Paste. *Journal of Materials in Civil Engineering* **2017**, *29* (9), 04017087. https://doi.org/10.1061/(ASCE)MT.1943-5533.0001926.

(22) Park, S.; Ruoff, R. S. Chemical Methods for the Production of Graphenes. *Nature Nanotech* **2009**, *4* (4), 217–224. https://doi.org/10.1038/nnano.2009.58.

(23) Mbayachi, V. B.; Ndayiragije, E.; Sammani, T.; Taj, S.; Mbuta, E. R.; khan, A. ullah. Graphene Synthesis, Characterization and Its Applications: A Review. *Results in Chemistry* **2021**, *3*, 100163. https://doi.org/10.1016/j.rechem.2021.100163.

(24) Viculis, L. M.; Mack, J. J.; Kaner, R. B. A Chemical Route to Carbon Nanoscrolls. *Science* **2003**, *299* (5611), 1361–1361. https://doi.org/10.1126/science.1078842.

(25) Mahmood, F.; Ashraf, S.; Shahzad, M.; Li, B.; Asghar, F.; Amjad, W.; Omar, M. M. Graphene Synthesis from Organic Substrates: A Review. *Ind. Eng. Chem. Res.* **2023**, *62* (42), 17314–17327. https://doi.org/10.1021/acs.iecr.3c01715.

(26) Guex, L. G.; Sacchi, B.; Peuvot, K. F.; Andersson, R. L.; Pourrahimi, A. M.; Ström, V.; Farris, S.; Olsson, R. T. Experimental Review: Chemical Reduction of Graphene Oxide (GO) to Reduced Graphene Oxide (rGO) by Aqueous Chemistry. *Nanoscale* **2017**, *9* (27), 9562–9571. https://doi.org/10.1039/C7NR02943H.

(27) Jia, C.; Pang, M.; Lu, Y.; Liu, Y.; Zhuang, M.; Liu, B.; Lu, J.; Wei, T.; Wang, L.; Bian, T.; Wang, M.; Yu, F.; Sun, L.; Lin, L.; Teng, T.; Wu, X.; He, Z.; Gao, J.; Luo, J.; Zhang, S.; Feng, L.; Yin, X.; You, F.; Li, G.; Zhang, L.; Zhu, Y.-G.; Zhu, X.; Yang, Y. Graphene Environmental Footprint Greatly Reduced When Derived from Biomass Waste via Flash Joule Heating. *One Earth* **2022**, *5* (12), 1394–1403. https://doi.org/10.1016/j.oneear.2022.11.006.

(28) Cossutta, M.; McKechnie, J.; Pickering, S. J. A Comparative LCA of Different Graphene Production Routes. *Green Chem.* **2017**, *19* (24), 5874–5884. https://doi.org/10.1039/C7GC02444D.

(29) Backes, C.; Abdelkader, A. M.; Alonso, C.; Andrieux-Ledier, A.; Arenal, R.; Azpeitia, J.; Balakrishnan, N.; Banszerus, L.; Barjon, J.; Bartali, R.; Bellani, S.; Berger, C.; Berger, R.; Ortega, M. M. B.; Bernard, C.; Beton, P. H.; Beyer, A.; Bianco, A.; Bøggild, P.; Bonaccorso, F.; Barin, G. B.; Botas, C.; Bueno, R. A.; Carriazo, D.; Castellanos-Gomez, A.; Christian, M.; Ciesielski, A.; Ciuk, T.; Cole, M. T.; Coleman, J.; Coletti, C.; Crema, L.; Cun, H.; Dasler, D.; Fazio, D. D.; Díez, N.; Drieschner, S.; Duesberg, G. S.; Fasel, R.; Feng, X.; Fina, A.; Forti, S.; Galiotis, C.; Garberoglio, G.; García, J. M.; Garrido, J. A.; Gibertini, M.; Gölzhäuser, A.; Gómez, J.; Greber, T.; Hauke, F.; Hemmi, A.; Hernandez-Rodriguez, I.; Hirsch, A.; Hodge, S. A.; Huttel, Y.; Jepsen, P. U.; Jimenez, I.; Kaiser, U.; Kaplas, T.; Kim, H.; Kis, A.; Papagelis, K.; Kostarelos, K.; Krajewska, A.; Lee, K.; Li, C.; Lipsanen, H.; Liscio, A.; Lohe, M. R.; Loiseau, A.; Lombardi, L.; López, M. F.; Martin, O.; Martín, C.; Martínez, L.; Martin-Gago, J. A.; Martínez, J. I.; Marzari, N.; Mayoral, Á.; McManus, J.; Melucci, M.; Méndez, J.; Merino, C.; Merino, P.; Meyer, A. P.; Miniussi, E.; Miseikis, V.; Mishra, N.; Morandi, V.; Munuera, C.; Muñoz, R.; Nolan, H.; Ortolani, L.; Ott, A. K.; Palacio, I.; Palermo, V.; Parthenios, J.; Pasternak, I.; Patane, A.; Prato, M.; Prevost, H.;

Prudkovskiy, V.; Pugno, N.; Rojo, T.; Rossi, A.; Ruffieux, P.; Samorì, P.; Schué, L.; Setijadi, E.; Seyller, T.; Speranza, G.; Stampfer, C.; Stenger, I.; Strupinski, W.; Svirko, Y.; Taioli, S.; Teo, K. B. K.; Testi, M.; Tomarchio, F.; Tortello, M.; Treossi, E.; Turchanin, A.; Vazquez, E.; Villaro, E.; Whelan, P. R.; Xia, Z.; Yakimova, R.; Yang, S.; Yazdi, G. R.; Yim, C.; Yoon, D.; Zhang, X.; Zhuang, X.; Colombo, L.; Ferrari, A. C.; Garcia-Hernandez, M. Production and Processing of Graphene and Related Materials. *2D Mater.* **2020**, *7* (2), 022001. https://doi.org/10.1088/2053-1583/ab1e0a.

(30) Wright, J. P.; Sigdel, S.; Corkill, S.; Covarrubias, J.; LeBan, L.; Nepal, A.; Li, J.; Divigalpitiya, R.; Bossmann, S. H.; Sorensen, C. M. Synthesis of Turbostratic Nanoscale Graphene via Chamber Detonation of Oxygen/Acetylene Mixtures. *Nano Select* **2022**, *3* (6), 1054–1068. https://doi.org/10.1002/nano.202100305.

(31) Munuera, J.; Britnell, L.; Santoro, C.; Cuéllar-Franca, R.; Casiraghi, C. A Review on Sustainable Production of Graphene and Related Life Cycle Assessment. *2D Mater.* **2021**, *9* (1), 012002. https://doi.org/10.1088/2053-1583/ac3f23.

(32) AMFadmin. *HydroGraph Achieves Critical Technology Milestone for the First Cost Effective Modular Commercial Scale Unit for Production of High-Purity Graphene*. HydroGraph. https://hydrograph.com/hydrograph-achieves-critical-technology-milestone-for-the-first-cost-effective-modular-commercial-scale-unit-for-production-of-high-purity-graphene/ (accessed 2024-02-06).

(33) Yan, Y.; Nashath, F. Z.; Chen, S.; Manickam, S.; Lim, S. S.; Zhao, H.; Lester, E.; Wu, T.; Pang, C. H. Synthesis of Graphene: Potential Carbon Precursors and Approaches. *Nanotechnology Reviews* **2020**, *9* (1), 1284–1314. https://doi.org/10.1515/ntrev-2020-0100.

(34) Nepal, A.; Singh, G. P.; Flanders, B. N.; Sorensen, C. M. One-Step Synthesis of Graphene via Catalyst-Free Gas-Phase Hydrocarbon Detonation. *Nanotechnology* **2013**, *24* (24), 245602. https://doi.org/10.1088/0957-4484/24/24/245602.

(35) Covarrubias, J. J. Rational Chemical Applications of Explosion-Graphene, Department of Chemistry College of Arts and Sciences , KANSAS STATE UNIVERSITY, Manhattan, Kansas, 2021. https://krex.k-state.edu/handle/2097/41627 (accessed 2024-01-23).

(36) Piñas, J. A. V.; Andrade, T. S.; Oliveira, A. T.; Salomão, P. E. A.; Rodriguez, M.; Silva, A. C.; Oliveira, H. S.; Monteiro, D. S.; Pereira, M. C. Production of Reduced Graphene Oxide Platelets from Graphite Flakes Using the Fenton Reaction as an Alternative to Harmful Oxidizing Agents. *Journal of Nanomaterials* **2019**, *2019*, e5736563. https://doi.org/10.1155/2019/5736563.

(37) Ye, T.; Yang, Y.; Bai, J.; Wu, F.-Y.; Zhang, L.; Meng, L.-Y.; Lan, Y. The Mechanical, Optical, and Thermal Properties of Graphene Influencing Its Pre-Clinical Use in Treating Neurological Diseases. *Frontiers in Neuroscience* **2023**, *17*.

(38) Chen, C.; Chen, T.; Wang, H.; Sun, G.; Yang, X. A Rapid, One-Step, Variable-Valence Metal Ion Assisted Reduction Method for Graphene Oxide. *Nanotechnology* **2011**, *22* (40), 405602. https://doi.org/10.1088/0957-4484/22/40/405602.

(39) Tamang, S.; Rai, S.; Bhujel, R.; Bhattacharyya, N. K.; Swain, B. P.; Biswas, J. A Concise Review on GO, rGO and Metal Oxide/rGO Composites: Fabrication and Their Supercapacitor and Catalytic Applications. *Journal of Alloys and Compounds* **2023**, *947*, 169588. https://doi.org/10.1016/j.jallcom.2023.169588.

(40) Salami, B. A.; Mukhtar, F.; Ganiyu, S. A.; Adekunle, S.; Saleh, T. A. Graphene-Based Concrete: Synthesis Strategies and Reinforcement Mechanisms in Graphene-Based Cementitious Composites (Part 1). *Construction and Building Materials* **2023**, *396*, 132296. https://doi.org/10.1016/j.conbuildmat.2023.132296.

(41) Murali, M.; Alaloul, W. S.; Mohammed, B. S.; Musarat, M. A.; Salaheen, M. A.; Al-Sabaeei, A. M.; Isyaka, A. Utilizing Graphene Oxide in Cementitious Composites: A Systematic Review. *Case Studies in Construction Materials* **2022**, *17*, e01359. https://doi.org/10.1016/j.cscm.2022.e01359.

(42) Stoller, M. D.; Park, S.; Zhu, Y.; An, J.; Ruoff, R. S. Graphene-Based Ultracapacitors. *Nano Lett.* **2008**, *8* (10), 3498–3502. https://doi.org/10.1021/nl802558y.

(43) Shi, X.; Zheng, S.; Wu, Z.-S.; Bao, X. Recent Advances of Graphene-Based Materials for High-Performance and New-Concept Supercapacitors. *Journal of Energy Chemistry* **2018**, *27* (1), 25–42. https://doi.org/10.1016/j.jechem.2017.09.034.

(44) Wang, G.; Yang, J.; Park, J.; Gou, X.; Wang, B.; Liu, H.; Yao, J. Facile Synthesis and Characterization of Graphene Nanosheets. *J. Phys. Chem. C* **2008**, *112* (22), 8192–8195. https://doi.org/10.1021/jp710931h.

(45) Sheng, Z.-H.; Shao, L.; Chen, J.-J.; Bao, W.-J.; Wang, F.-B.; Xia, X.-H. Catalyst-Free Synthesis of Nitrogen-Doped Graphene via Thermal Annealing Graphite Oxide with Melamine and Its Excellent Electrocatalysis. *ACS Nano* **2011**, *5* (6), 4350–4358. https://doi.org/10.1021/nn103584t.

(46) Goldie, S. J.; Bush, S.; Cumming, J. A.; Coleman, K. S. A Statistical Approach to Raman Analysis of Graphene-Related Materials: Implications for Quality Control. *ACS Appl. Nano Mater.* **2020**, *3* (11), 11229–11239. https://doi.org/10.1021/acsanm.0c02361.

(47) Arora, A.; Aguayo, M.; Hansen, H.; Castro, C.; Federspiel, E.; Mobasher, B.; Neithalath, N. Microstructural Packing- and Rheology-Based Binder Selection and Characterization for Ultra-High Performance Concrete (UHPC). *Cement and Concrete Research* **2018**, *103*, 179–190. https://doi.org/10.1016/j.cemconres.2017.10.013.

(48) Surehali, S.; Simon, A.; Ramasamy, R. K.; Neithalath, N. A Comparison of the Effect of Activator Cations (Sodium and Potassium) on the Fresh and Hardened Properties of Mine Tailing-Slag Binders. *Construction Materials* **2023**, *3* (4), 389–404. https://doi.org/10.3390/constrmater3040025.

(49) Marsh, B. K.; Day, R. L. Pozzolanic and Cementitious Reactions of Fly Ash in Blended Cement Pastes. *Cement and Concrete Research* **1988**, *18* (2), 301–310. https://doi.org/10.1016/0008-8846(88)90014-2.

(50) Zeng, Q.; Li, K.; Fen-chong, T.; Dangla, P. Determination of Cement Hydration and Pozzolanic Reaction Extents for Fly-Ash Cement Pastes. *Construction and Building Materials* **2012**, *27* (1), 560–569. https://doi.org/10.1016/j.conbuildmat.2011.07.007.

(51) Aguayo, M.; Yang, P.; Vance, K.; Sant, G.; Neithalath, N. Electrically Driven Chloride Ion Transport in Blended Binder Concretes: Insights from Experiments and Numerical Simulations. *Cement and Concrete Research* **2014**, *66*, 1–10. https://doi.org/10.1016/j.cemconres.2014.07.022.

(52) Surehali, S.; Tripathi, A.; Nimbalkar, A. S.; Neithalath, N. Anisotropic Chloride Transport in 3D Printed Concrete and Its Dependence on Layer Height and Interface Types. *Additive Manufacturing* **2023**, *62*, 103405. https://doi.org/10.1016/j.addma.2023.103405.

(53) Wang, W.; Wang, B.; Zhang, S. Dispersion, Properties, and Mechanisms of Nanotechnology-Modified Alkali-Activated Materials: A Review. *Renewable and Sustainable Energy Reviews* **2024**, *192*, 114215. https://doi.org/10.1016/j.rser.2023.114215.

(54) Long, W.-J.; Gu, Y.; Xing, F.; Khayat, K. H. Microstructure Development and Mechanism of Hardened Cement Paste Incorporating Graphene Oxide during Carbonation. *Cement and Concrete Composites* **2018**, *94*, 72–84. https://doi.org/10.1016/j.cemconcomp.2018.08.016.

(55) Long, W.-J.; Wei, J.-J.; Xing, F.; Khayat, K. H. Enhanced Dynamic Mechanical Properties of Cement Paste Modified with Graphene Oxide Nanosheets and Its Reinforcing Mechanism. *Cement and Concrete Composites* **2018**, *93*, 127–139. https://doi.org/10.1016/j.cemconcomp.2018.07.001.

(56) Li, W.; Li, X.; Chen, S. J.; Liu, Y. M.; Duan, W. H.; Shah, S. P. Effects of Graphene Oxide on Early-Age Hydration and Electrical Resistivity of Portland Cement Paste. *Construction and Building Materials* **2017**, *136*, 506–514. https://doi.org/10.1016/j.conbuildmat.2017.01.066.

(57) Liu, B.; Wang, L.; Pan, G.; Li, D. Dispersion of Graphene Oxide Modified Polycarboxylate Superplasticizer in Cement Alkali Solution for Improving Cement Composites. *Journal of Building Engineering* **2022**, *57*, 104860. https://doi.org/10.1016/j.jobe.2022.104860.

(58) Ho, V. D.; Ng, C.-T.; Ozbakkaloglu, T.; Karunagaran, R. U.; Farivar, F.; Goodwin, A.; Guckin, C. M.; Ho, V. D.; Losic, D. Investigating the Reinforcing Mechanism and Optimized Dosage of Pristine Graphene for Enhancing Mechanical Strengths of Cementitious Composites. *RSC Adv.* **2020**, *10* (70), 42777–42789. https://doi.org/10.1039/D0RA07639B.

(59) Wang, B.; Shuang, D. Effect of Graphene Nanoplatelets on the Properties, Pore Structure and Microstructure of Cement Composites. *Materials Express* **2018**, *8* (5), 407–416. https://doi.org/10.1166/mex.2018.1447.

(60) Liu, J.; Fu, J.; Yang, Y.; Gu, C. Study on Dispersion, Mechanical and Microstructure Properties of Cement Paste Incorporating Graphene Sheets. *Construction and Building Materials* **2019**, *199*, 1–11. https://doi.org/10.1016/j.conbuildmat.2018.12.006.

(61) Wang, B.; Pang, B. Mechanical Property and Toughening Mechanism of Water Reducing Agents Modified Graphene Nanoplatelets Reinforced Cement Composites. *Construction and Building Materials* **2019**, *226*, 699–711. https://doi.org/10.1016/j.conbuildmat.2019.07.229.

(62) Sheikh, T. M.; Anwar, M. P.; Muthoosamy, K.; Jaganathan, J.; Chan, A.; Mohamed, A. A. The Mechanics of Carbon-Based Nanomaterials as Cement Reinforcement — A Critical Review. *Construction and Building Materials* **2021**, *303*, 124441. https://doi.org/10.1016/j.conbuildmat.2021.124441.

(63) Zeng, H.; Qu, S.; Tian, Y.; Hu, Y.; Li, Y. Recent Progress on Graphene Oxide for Next-Generation Concrete: Characterizations, Applications and Challenges. *Journal of Building Engineering* **2023**, *69*, 106192. https://doi.org/10.1016/j.jobe.2023.106192.

(64) Zhao, L.; Guo, X.; Ge, C.; Li, Q.; Guo, L.; Shu, X.; Liu, J. Investigation of the Effectiveness of PC@GO on the Reinforcement for Cement Composites. *Construction and Building Materials* **2016**, *113*, 470–478. https://doi.org/10.1016/j.conbuildmat.2016.03.090.

(65) Rhee, I.; Lee, J. S.; Kim, Y. A.; Kim, J. H.; Kim, J. H. Electrically Conductive Cement Mortar: Incorporating Rice Husk-Derived High-Surface-Area Graphene. *Construction and Building Materials* **2016**, *125*, 632–642. https://doi.org/10.1016/j.conbuildmat.2016.08.089.

(66) Rhee, I.; Kim, Y. A.; Shin, G.-O.; Kim, J. H.; Muramatsu, H. Compressive Strength Sensitivity of Cement Mortar Using Rice Husk-Derived Graphene with a High Specific Surface Area. *Construction and Building Materials* **2015**, *96*, 189–197. https://doi.org/10.1016/j.conbuildmat.2015.08.016.

(67) Cao, M.; Zhang, H.; Zhang, C. Effect of Graphene on Mechanical Properties of Cement Mortars. *J. Cent. South Univ.* **2016**, *23* (4), 919–925. https://doi.org/10.1007/s11771-016-3139-4.

(68) Zhao, L.; Guo, X.; Ge, C.; Li, Q.; Guo, L.; Shu, X.; Liu, J. Mechanical Behavior and Toughening Mechanism of Polycarboxylate Superplasticizer Modified Graphene Oxide Reinforced Cement Composites. *Composites Part B: Engineering* **2017**, *113*, 308–316. https://doi.org/10.1016/j.compositesb.2017.01.056.

(69) Nair, S. A. O.; Panda, S.; Santhanam, M.; Sant, G.; Neithalath, N. A Critical Examination of the Influence of Material Characteristics and Extruder Geometry on 3D Printing of Cementitious Binders. *Cement and Concrete Composites* **2020**, *112*, 103671. https://doi.org/10.1016/j.cemconcomp.2020.103671.

(70) Alghamdi, H.; Nair, S. A. O.; Neithalath, N. Insights into Material Design, Extrusion Rheology, and Properties of 3D-Printable Alkali-Activated Fly Ash-Based Binders. *Materials & Design* **2019**, *167*, 107634. https://doi.org/10.1016/j.matdes.2019.107634.

(71) Rehman, S. K. U.; Ibrahim, Z.; Jameel, M.; Memon, S. A.; Javed, M. F.; Aslam, M.; Mehmood, K.; Nazar, S. Assessment of Rheological and Piezoresistive Properties of Graphene Based Cement Composites. *International Journal of Concrete Structures and Materials* **2018**, *12* (1), 64. https://doi.org/10.1186/s40069-018-0293-0.

(72) Shang, Y.; Zhang, D.; Yang, C.; Liu, Y.; Liu, Y. Effect of Graphene Oxide on the Rheological Properties of Cement Pastes. *Construction and Building Materials* **2015**, *96*, 20–28. https://doi.org/10.1016/j.conbuildmat.2015.07.181.

(73) Li, H.; Ding, S.; Zhang, L.; Ouyang, J.; Han, B. Rheological Behaviors of Cement Pastes with Multi-Layer Graphene. *Construction and Building Materials* **2021**, *269*, 121327. https://doi.org/10.1016/j.conbuildmat.2020.121327.

(74) Grzeszczyk, S.; Lipowski, G. Effect of Content and Particle Size Distribution of High-Calcium Fly Ash on the Rheological Properties of Cement Pastes. *Cement and Concrete Research* **1997**, *27* (6), 907–916. https://doi.org/10.1016/S0008-8846(97)00073-2.

(75) Bentz, D. P.; Ferraris, C. F.; Galler, M. A.; Hansen, A. S.; Guynn, J. M. Influence of Particle Size Distributions on Yield Stress and Viscosity of Cement–Fly Ash Pastes. *Cement and Concrete Research* **2012**, *42* (2), 404–409. https://doi.org/10.1016/j.cemconres.2011.11.006.

(76) Kumar, A.; Oey, T.; Falzone, G.; Huang, J.; Bauchy, M.; Balonis, M.; Neithalath, N.; Bullard, J.; Sant, G. The Filler Effect: The Influence of Filler Content and Type on the Hydration Rate of Tricalcium Silicate. *Journal of the American Ceramic Society* **2017**, *100* (7), 3316–3328. https://doi.org/10.1111/jace.14859.

(77) Oey, T.; Kumar, A.; Bullard, J. W.; Neithalath, N.; Sant, G. The Filler Effect: The Influence of Filler Content and Surface Area on Cementitious Reaction Rates. *Journal of the American Ceramic Society* **2013**, *96* (6), 1978–1990. https://doi.org/10.1111/jace.12264.

(78) Meng, S.; Ouyang, X.; Fu, J.; Niu, Y.; Ma, Y. The Role of Graphene/Graphene Oxide in Cement Hydration. *Nanotechnology Reviews* **2021**, *10* (1), 768–778. https://doi.org/10.1515/ntrev-2021-0055.

(79) Sanchez, F.; Zhang, L. Molecular Dynamics Modeling of the Interface between Surface Functionalized Graphitic Structures and Calcium–Silicate–Hydrate: Interaction Energies, Structure, and Dynamics. *Journal of Colloid and Interface Science* **2008**, *323* (2), 349–358. https://doi.org/10.1016/j.jcis.2008.04.023.

(80) Das, S.; Aguayo, M.; Dey, V.; Kachala, R.; Mobasher, B.; Sant, G.; Neithalath, N. The Fracture Response of Blended Formulations Containing Limestone Powder: Evaluations Using Two-Parameter Fracture Model and Digital Image Correlation. *Cement and Concrete Composites* **2014**, *53*, 316–326. https://doi.org/10.1016/j.cemconcomp.2014.07.018.

(81) Arvidsson, R.; Kushnir, D.; Sandén, B. A.; Molander, S. Prospective Life Cycle Assessment of Graphene Production by Ultrasonication and Chemical Reduction. *Environ. Sci. Technol.* **2014**, *48* (8), 4529–4536. https://doi.org/10.1021/es405338k.

(82) Ciroth, A.; Di Noi, C.; Lohse, T.; Srocka, M. openLCA 1.10 Comprehensive User Manual. *GreenDelta, Berlin, Germany* **2020**.

(83) Simon, A.; Tripathi, A.; Surehali, S.; Neithalath, N. Carpet Fiber Recycling in Regular-Use Concrete Mixtures and Associated Life Cycle Analysis. *Waste Management Bulletin* **2023**, *1* (3), 103–114. https://doi.org/10.1016/j.wmb.2023.07.005.

(84) Ryberg, M.; Vieira, M. D. M.; Zgola, M.; Bare, J.; Rosenbaum, R. K. Updated US and Canadian Normalization Factors for TRACI 2.1. *Clean Techn Environ Policy* **2014**, *16* (2), 329–339. https://doi.org/10.1007/s10098-013-0629-z.

For Table of Contents Use Only:

Description:

Novel graphenes reported in this study provide dual sustainability benefits: (i) graphene production with significantly lower environmental impacts, and (ii) very small amounts of graphene (~0.02% by weight of cement) results in improved properties and sustainability metrics of cementitious binders.

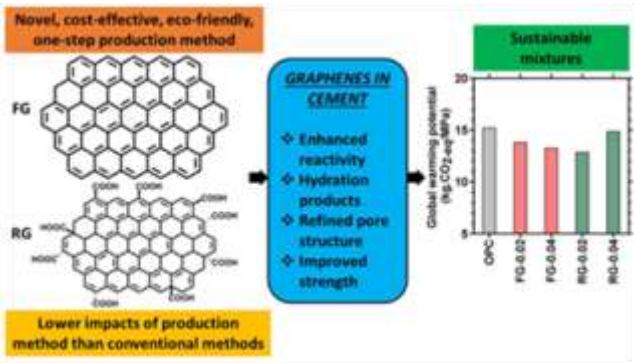

Figure 1: Table of Contents (TOC) graphic